Original article
doi: 10.17223/25421379/24/9

FLOOD MONITORING APPLICATION OF 2018 LAOS DAM COLLAPSE BASED ON SENTINEL-1A SAR DATA AND THE OBJECT-ORIENTED METHOD

Jun Ma[1], Vadim V. Khromykh[2], Anna A. Chekina[3]

[1, 2, 3] *National Research Tomsk State University, Tomsk, Russia*
[1] *majun6982@gmail.com*
[2] *khromykh_vadim@mail.ru*
[3] *chekina.ann@gmail.com*

Abstract. Flood disasters seriously threaten the survival and development of human beings. Monitoring the changes of water bodies during floods and estimating the affected area is essential for comprehensive and accurate analysis of disaster information. Recently, radar satellite data has been increasingly used for flood monitoring, since in this case, cloudiness is not an obstacle to estimating the flood area. In this paper Sentinel-1 ground range detected (GRD) data was selected to estimate the inundated area after the Xe-Pian Xe-Namnoy Dam breach in Laos at the end of July 2018. The flooded Hinlat area and the Xe-Pian Xe-Namnoy reservoir were selected as the study area for flood inundation extent monitoring, because this area is characterized by bare land, agricultural land, and residential land with complex topography and geomorphology. The study area is located in the Bolaven Plateau, is a highland region in southern Laos. One of the reasons for the flooding of the study area is an elevation difference between upper reaches and downstream of the river. Several reaches with a convex profile and knickpoints because of the geologic control when draining the plateau represent the undeveloped longitudinal profile of the Vang Ngao River. The main channel of the Vang Ngao River is dug into Mesozoic fluvial sandstones, which resist scouring by the flood. The eCognition software is used to organize the process of extracting information about the flood zone. The object-oriented approach and the threshold method are combined to extract information about the reservoir. First, SNAP software is used to pre-process Sentinel-1A SAR images. Then, the eCognition multi-scale segmentation method is used to determine the best segmentation scale, for iterative testing and comparative analysis of experimental results, taking into account the characteristics of the object and a priori knowledge. After sensitivity analysis of the flooded area image features and other features, the VH-polarized backscattered mean features were selected to construct a knowledge base for flooded area extraction to differentiate water and non-water bodies. At the same time, the modified bare soil index (MBI) and the terrain relief were combined to remove the influence of bare land and mountain shadow on the extraction results to achieve the 2018 dam collapse flood monitoring in Laos. Finally, the extent and area of the affected region were analyzed and the changes of water bodies before and after the disaster were mapped. The study shows that the monitoring results of Sentinel-1A SAR data are more consistent with the actual situation and have significant advantages in flood hazard monitoring and assessment, which can effectively carry out large-scale flood inundation extent monitoring.

Keywords: *remote sensing, Sentinel-1A SAR, object-oriented method, change detection, flood, geomorphology, Laos*

Source of financing: *The reported study was funded by RFBR, project number 20-35-90085.*

For citation: Ma Jun, Khromykh V.V., Chekina A.A. (2022) Flood monitoring application of 2018 Laos dam collapse based on Sentinel-1a SAR data and the object-oriented method. *Geosfernye issledovaniya – Geosphere Research*. 3. pp. 136–147. (In Russian). doi: 10.17223/25421379/24/9

Научная статья
УДК 528.8
doi: 10.17223/25421379/24/9

ПРИЛОЖЕНИЕ ДЛЯ МОНИТОРИНГА ЗАТОПЛЕНИЯ ТЕРРИТОРИИ ПРИ ОБРУШЕНИИ ПЛОТИНЫ В ЛАОСЕ В 2018 г. НА ОСНОВЕ ДАННЫХ SAR SENTINEL-1A И ОБЪЕКТНО-ОРИЕНТИРОВАННОГО МЕТОДА

Дзюнь Ма[1], Вадим Валерьевич Хромых[2], Анна Александровна Чекина[3]

[1, 2, 3] *Национальный исследовательский Томский государственный университет, Томск, Россия*
[1] *majun6982@gmail.com*
[2] *khromykh_vadim@mail.ru*
[3] *chekina.ann@gmail.com*

Аннотация. Стихийные бедствия, такие как наводнения, представляют серьезную угрозу жизнедеятельности и развитию человеческого общества, а также окружающей среде. Чтобы выполнить комплексный анализ данного

природного явления и в дальнейшем предупредить его, возникает потребность в мониторинге динамики водоемов в период наводнений и оценке риска уязвимых территорий. В настоящее время для мониторинга наводнений часто используются радиолокационные спутниковые данные, поскольку они позволяют точно оценить площади затапливаемых участков, несмотря на наличие облачности в атмосфере. Для оценки площади затопления территорий в результате прорыва дамбы Xe-Pian Xe-Namnoy (Лаос) в конце июля 2018 г. были использованы данные, спроецированные на наземную дальность с использованием модели земного эллипсоида. В качестве района исследований выбран населенный пункт Хинлат и водохранилище Xe-Pian Xe-Namnoy, которые располагаются на плато Боловен в южной части Лаоса и характеризуются сложной геоморфологической структурой, наличием сельскохозяйственных угодий и жилой застройки. В гидрологическом отношении район испытывает влияние реки Ванг Нгао с невыработанным продольным профилем русла, которое врезано в мезозойские песчаники, устойчивые к размыву. Перепад высот между верхним и нижним течением реки является одной из причин затопления исследуемой территории. Чтобы организовать процесс получения данных о затоплении со спутниковых снимков, были выбраны снимки SAR Sentinel-1A и использовано программное обеспечение eCognition, объектно-ориентированный подход и пороговый метод обработки изображений. Предварительная обработка снимков выполнена при помощи программы SNAP, после чего был применен метод многомасштабной сегментации изображений с целью провести итеративное тестирование и сравнить характеристики затопленных территорий. Наряду с сегментацией был учтен измененный индекс участков без растительности (MBI) в сочетании с характеристиками рельефа, чтобы исключить влияние поверхности этих участков и теней рельефа на результаты извлечения. В результате сравнительного анализа выбраны усредненные характеристики VH-поляризованного обратного рассеяния для выделения затопленных зон с возможностью отличить водные объекты от других, неводных. Далее был проведен анализ площади затопления изучаемого района с последующим моделированием динамики водных объектов до и после стихийного бедствия. Таким образом, результаты исследования показали, что данные SAR Sentinel-1A соответствуют реальной ситуации и обладают преимуществами при решении задач мониторинга наводнений и оценки площади их распространения.

Ключевые слова: *дистанционное зондирование Земли, Sentinel-1A SAR, объектно-ориентированный подход, метод «change detection», наводнение, геоморфология, Лаос*

Источник финансирования: *исследование выполнено при финансовой поддержке РФФИ в рамках научного проекта № 20-35-90085.*

Для цитирования: Ma J., Khromykh V.V., Chekina A.A. Flood monitoring application of 2018 Laos dam collapse based on Sentinel-1a SAR data and the object-oriented method // Геосферные исследования. 2022. № 3. С. 136–147. doi: 10.17223/25421379/24/9

Introduction

Flood disaster is one of the most destructive sudden disasters globally and has a short duration and great danger. Flood disasters affect a wide area and cause severe losses, posing a significant threat to the safety of people's lives and property and the economic development of the affected areas [Domeneghetti, Schumann, Tarpanelli, 2019]. The inundation of large areas caused by flash floods is dynamic, and real-time monitoring of flooded areas is necessary. Based on 3S technologies of remote sensing (RS), geographic information system (GIS) technology, global satellite navigation (GPS) technology, and their cooperation, we can achieve fast and accurate extraction of inundation area, visualize its spatial distribution, dynamic change and development pattern, and provide a reference for flood disaster monitoring and assessment work. Since the end of the 20th century, the development and application of remote sensing technology have provided a new alternative. NOAA [Jain et al., 2006], MODIS [Sakamoto et al., 2007], Aster [Khromykh, Khromykh, 2016, 2018], Landsat MSS [Sharitz, 1986], Landsat TM [McFeeters, 1996], Landsat 8 [Nandi, Srivastava, Shah, 2017] and other optical remote sensing images are used to monitor the floodplain landscapes and extract the area of flooding occurrence. However, when flooding occurs, the disaster area often lasts for a long time with cloudy weather and covers many clouds. The temporal resolution and spatial resolution of optical remote sensing images are mutually constrained. Due to the wavelength characteristics of the used bands, they are easily affected by clouds and weather, which makes the monitoring results inaccurate, time-sensitive, and challenging to reflect the actual situation of the disaster area.

Synthetic aperture radar (SAR) selected waveband has the advantages of all-weather, all-day working capability and vast area coverage and observation. It is not affected by clouds, rain, and fog, especially suitable for flood inundation range monitoring [Schlaffer et al., 2015]. Furthermore, on the SAR image, the specular reflection of the water body appears as a dark tone on the image and the information of the water body is elementary to be identified [Tang et al., 2018]. Therefore, SAR can be an essential complement to optical remote sensing satellite monitoring on cloudy days. With the continuous development of SAR technology, radar remote sensing data in natural disaster monitoring has been dramatically developed. Wood et al. [2018] used the latest SAR image data to achieve higher accuracy

flood monitoring. Hess et al. [1995] experimentally demonstrated that SAR data could effectively identify information about water bodies mixed with vegetation and other disturbing features. Kiage and Walker [2005] demonstrated that Radarsat-1ScanSAR data is well suited for water body monitoring. Moreover, Ramsey et al. [2011] demonstrated the difference in the reflection of water body information by SAR image data with different polarization types. Numerous scholars have made many efforts to make these data sources widely used and have contributed significantly to the development of SAR imagery for regional flood monitoring. ESA's Copernicus satellite Sentinel-1A can provide high-resolution SAR images for timely, continuous, and independent emergency response to natural disasters, providing essential data support for flood monitoring and assessment of inundation extent during floods.

In this paper, we select Sentinel-1 ground range detected (GRD) data of the inundated area after the Xe-Pian Xe-Namnoy Dam breach in Laos in late July 2018. We use an object-oriented approach to create a process, which provides an extraction of inundation extent. The process gives quickly obtaining the inundation area and range before and after the occurrence of floods.

The study results lay the foundation for the operational extension of flood monitoring and assessment and provide a reference for the extending of this data in other application areas in the future.

Study area and data

Overview of the disaster area. On the night of July 23, 2018, a severe dam failure occurred at the Xe-Pian Xe-Namnoy reservoir's secondary dam D in the province of Azusa, Laos, releasing 500 million cubic meters of floodwater. The severe flooding submerged villages and the downstream, killing 98 people, leaving hundreds missing, and leaving more than 6,600 villagers homeless [Cheng, Zhao, Yin, 2019].

The flooded Hinlat area and the Xe-Pian Xe-Namnoy reservoir were selected as the study area for flood inundation extent monitoring, because this area is characterized by bare land, agricultural land, and residential land with complex topography and geomorphology (Fig. 1).

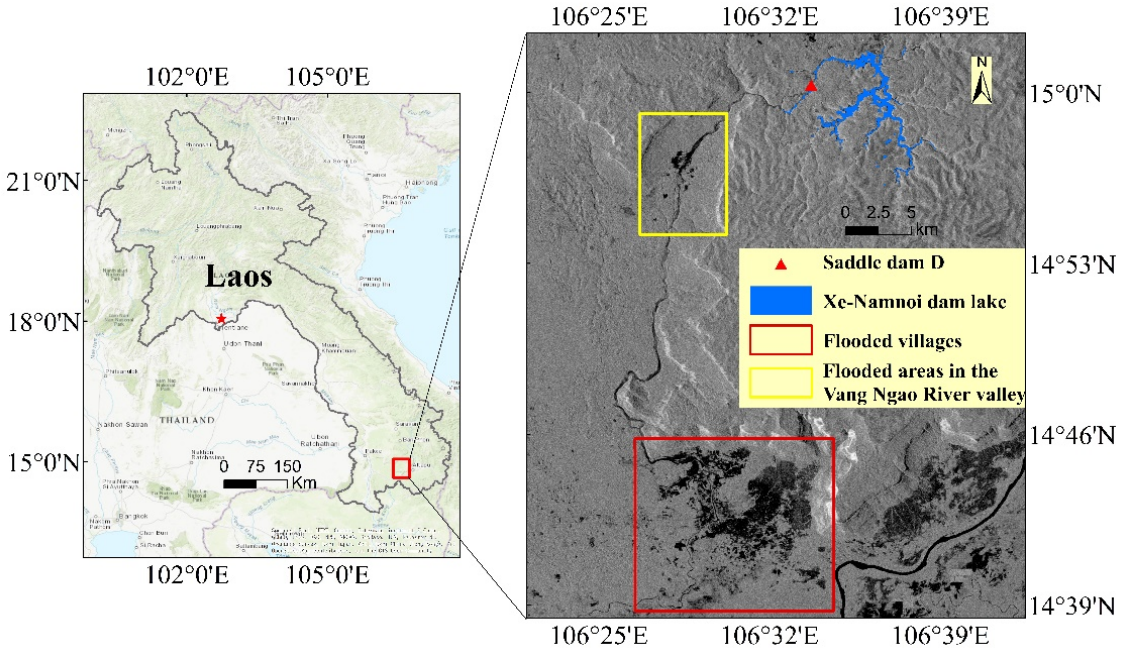

Fig. 1. Study area in the southwest of the Bolaven Plateau, Laos

Рис. 1. Район исследования на юго-западе плато Боловен, Лаос

The study area is located in the Bolaven Plateau, is a highland region in southern Laos. The plateau is framed by the Annamite Mountain Range to the south and east, and by the Mekong River valley to the north and west. The areal extent of the Bolaven Plateau is approximately 6,000 km^2 [Delang, Toro, 2011]. The gradient between the plateau and the surrounding landscape makes it an easily distinguishable topographic feature. The plateau is characterized by a relatively flat surface ranging from 1,000 to 1,350 m above sea level (ASL) [Latrubesse et al., 2020].

An orographic structure of the Bolaven is volcanic plateau. The basement of the plateau consists of the Tri-

assic-Cretaceous clastic sedimentary strata. Mesozoic quartz sandstones and fluvial/lacustrine mudstones underlie this elevated surface and crop out almost continuously around its cliffy perimeter. The nearly vertical pitches at the top of this perimeter cliff and from outcrops on the plateau indicate the uppermost 200–250 m of the Mesozoic bedrock comprise massive to cross-bedded fluvial sandstones. Gentler slopes below point to friable mudstones dominate the underlying 250 m [Sieh et al., 2020].

The surface is covered by quaternary basaltic lavas that have erupted through thick flat-lying Mesozoic rocks. The spillover and eruption of these basalts began in the Late Pleistocene, ended in the Early Pleistocene. Thickness of the volcanic field ranges from about 350 m at its peak to a few meters on its perimeters [Ouyang et al., 2019]. There are volcanic landforms on the plateau surface – scoria cones, which accounts to nearly 100 visible ones. In the present, the volcanic field is still active, as evidenced by the age of basaltic flows, which many are 100,000 years [Latrubesse et al., 2020].

The interior of the plateau is quasi-plain with the low mountain, hill, residual hill and hillock. It has a lower height difference and a smaller slope compared to its framing as cliffs and canyon landforms. [Ouyang et al., 2019]. Surrounding areas of Bolaven plateau presented as flat lands approximately 200–500 m ASL. In some cases, the terrain rises gradually or abruptly to a relatively flat surface, ranging in most areas about 800–1,400 m ASL. The highest peak of the Bolaven is located in its northeast and is about 1,704 m ASL. Notably, the plateau's morphology is the slight drop in elevation, which follows parts of the Xe Katam, Xe Namnoy and Xe Pian rivers, and divides Bolaven into two separate tablelands [Delang, Toro, 2011].

Climatic conditions of the study area belong to the typical tropical monsoon climate, with the wet season from May to October and a dry season from November to April. The coldest month of the year is January, with an average air minimum temperature 19 °C and maximum 30 °C. The hottest month is April, with an average low of 25 °C and high of 35 °C (Attapu province). The average wind speed is approximately 0.2–0.9 m/s. [https://weatherspark.com]. Heavy frequent rainstorms are concentrated, intense and widespread. Annual precipitation averages approximately 3,800 mm [Latrubesse et al., 2020]. According to meteorological data from the Global Precipitation Measurement (GPM) dataset, a substantial rainfall of 438 mm was recorded on July 22, 2018, with continuous rainfall weather and under the continuous influence of El Niño stream.

The hydrology of the region is presented by a relatively developed surface water system. The Bolaven Plateau is located in the Lower Mekong River basin. The surface is drained by left-bank tributaries of the Mekong as the Xe-Don, the Vang Ngao and the Xe-Khong Rivers. The tributaries are highly seasonal, with spikes of high flow rising from a low stage immediately following rainfall. The left-bank tributaries, drained to the high-rainfall areas of Laos, contribute to the major wet-season flows. Thus, the flow contributions for mainstream from the Mekong left bank (Pakse-Stung Treng river reach) is about 23 % [Campbell, 2009].

The plateau's rivers are under the influence of a differential erosion process, ongoing through the lava flows of diverse ages and thickness, and through the underlying Mesozoic sedimentary rocks. The rivers are incised, confined, and present knickpoints along the longitudinal profile, with rapids and waterfalls [Latrubesse et al., 2020].

One of the reasons for the flooding of the study area is an elevation difference between upper reaches and downstream of the river (Fig. 2).

The undeveloped longitudinal profile of the Vang Ngao River is represented by several reaches with a convex profile and knickpoints because of the geologic control when draining the plateau. The main channel of the Vang Ngao River is dug into Mesozoic fluvial sandstones, which resist scouring by the flood. Imagine a drainpipe made of metal material perpendicular to the surface. Rainwater comes there from above, and this flow is concentrated in the pipe, like a river in the rock-controlled channel. When the flow in the pipe reaches its end, the water spills over the ground.

Thus, the peculiar relief and high gradient of the riverbed in some sites (from 0.0107 to 0.0208) had an impact on the increasing of the water flow energy. Water flow velocities on steep sections of the flood path reached levels as high as approximately 12 m/s. As the result, a rapid flood propagation downstream, to the low-relief plain of Quaternary fluvial deposits, where the Hinlat area is located, was provided. The riverbed gradient decreases to the plain and forms a narrow floodplain with a channel incised approximately 6–7 m into alluvial sediment. Maximum floodplain inundation depth was approximately 9.5 m, although the channel capacity is approximately 5 m [Latrubesse et al., 2020].

Sentinel-1ASAR images. Sentinel-1A was launched in April 2014, with an orbital period of 12 days for a single satellite and a regular repeat period of 6 days for two satellites, with the fastest revisit time of 1 to 3 days. This satellite carries a 5,404 GHz C-band SAR with maximum coverage of 400 km, including four imaging modes: SM (Stripmap), IW (Interferometric Wide-swath), EW (Extra-Wideswath), and WV (Wave). The SM, IW, and EW modes are unipolar (HH/VV) and dual-polarized (HH+HV/VV+VH) imaging and the WV mode is unipolar (HH/VV) imaging [ESA, 2014]. Senti-

nel-1A SAR image is not affected by extreme weather, it can penetrate through clouds and acquire data with all-weather and wide coverage area. The acquired image has good contrast and rich texture information, which is especially suitable for the study and monitoring of sudden-onset disasters.

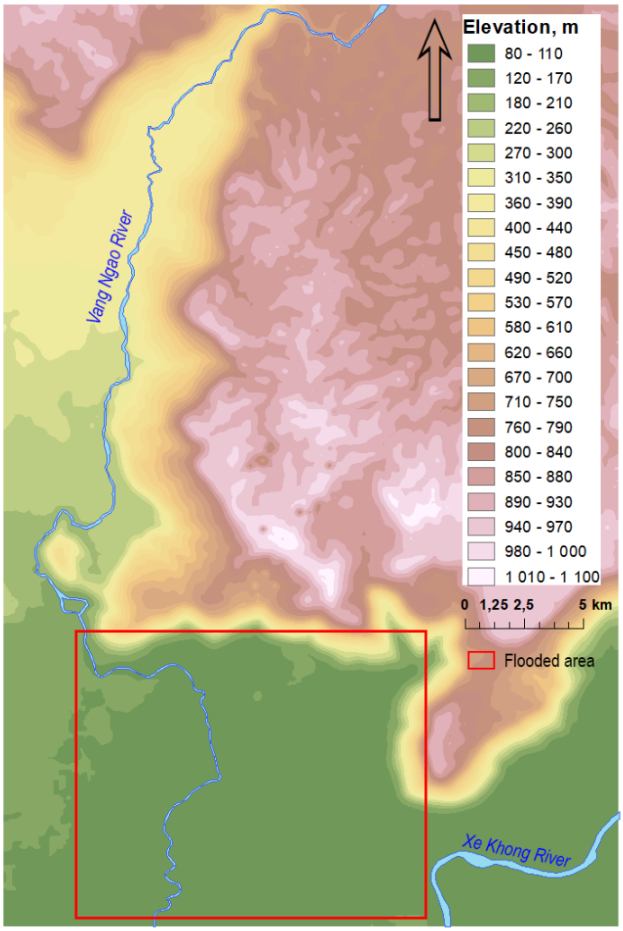

Fig. 2. The hypsometric map of the southwest part of the Bolaven Plateau

Рис. 2. Гипсометрическая карта юго-западной части плато Боловен

Moreover, in this image, the specular reflection phenomenon of the water body appears in dark tones, so the information of the water body can be simply identified. In this paper, the images of Sentinel-1A SAR before the flood outbreak on July 13, 2018, and after the flood outbreak on July 25, 2018, were selected for the extraction and analysis of the Xe-Pian Xe-Namnoy reservoir and the flooded area. The product level of this data is GRD (Ground Range Detected Product), the operating mode is IW, the polarization mode is VH, and the parameters of Sentinel-1A SAR data are shown in the table 1.

Table 1

Characteristics of processed Sentinel-1A images

Таблица 1

Характеристики снимков Sentinel-1A после предварительной обработки

Imaging date	Polarization mode	Resolution/m	Pixel size/m
2018/7/13 (Before the disaster)	VV/VH	20 × 22	10 × 10
2018/7/25 (After the disaster)	VV/VH	20 × 22	10 × 10

Geographic information data. In addition to SAR images, this paper also collected Landsat 8 remote sensing images of the same period in the study area. Digital elevation model (DEM) data and administrative division vector data were also collected. These data are used to assist the interpretation analysis of flooded areas and improve extraction accuracy. Among them, Landsat 8 remote sensing image is from USGS [https://earthexplorer.usgs.gov/], and DEM data is ALOS (Advanced Land Observing Satellite) with resolution 12.5 m. DEM data is the phased-array type L-band data. Synthetic Aperture Radar (PALSAR) acquired elevation data (https://earthdata.nasa.gov/). The administrative zoning vector data were obtained from WWF (https://www.worldwildlife.org/).

Research method

Pre-processing of Sentinel-1A images. In this study, the Sentinel-1A data were pre-processed using ESA SNAP software [Sun et al., 2017]. The primary process includes the following steps:

1. Orbit correction. The accuracy of the orbit state data in the metadata files accompanying the Sentinel-1 satellite data is not very high, as accurate orbit files usually take about two weeks after data acquisition to be produced [Guo, Zhao, 2018]. The SNAP software automatically downloads the exact orbit file and updates the Sentinel-1 satellite orbit status information in the metadata file (.xml) in the Sentinel-1 satellite data [Zhang et al., 2021]. In general, more precise orbital positions should be updated, especially when a higher level of alignment processing is required.

2. Thermal noise removal. The operating mode of SAR is active survey, and the Sentinel-1 satellite is about 700 km above ground level. Due to the wave spherical diffusion effect, the thermal loss inside the SAR satellite unit (transmitter, power amplifier, and receiver) is not negligible. Thus, it seems that the acquired SAR images are with thermal noise, and the thermal noise will affect the estimated accuracy of the acquired radar backscatter signal. However, everything is relative; if we receive a SAR effective signal much stronger than the thermal noise, the thermal noise effect can be neglected. For the Sentinel-1 satellite, this is an optional pre-processing operation.

3. Radiation calibration. Radiometric calibration is the conversion of the received backscattered signal into a physical quantity with units. In order to eliminate systematic and random radiometric distortions or aberrations generated during data acquisition and transmission, the radiometric correction of the image data for each period is performed using the radiometric correction tool (Calibrate) of the SNAP data processing software to obtain the radar backscattered coefficients for each period of the subsurface.

4. Speckle filtering. Speckle noise in SAR images is a principle drawback inherent to all imaging systems based on the coherence principle [Han, Guo, Wang, 2002]. Speckle noise in SAR images is generated in the radar echo signal, which severely affects the accuracy of information extraction. There are various filters to remove coherent speckle, aiming to reduce the effect of noise on image interpretation and improve the accuracy of water extraction. The most popular Refined Lee filter (improved Lee filter) is used here. It is an adaptive filter, and the filter window can be automatically adjusted according to the region. The algorithm filters out the coherent spot noise while keeping the edge information of the feature as well. Besides, it can reduce the bright and dark spots caused by the undulation of the water surface to a certain extent, which facilitates the recognition of water body information [Xu, Zhou, 2013].

5. Terrain correction. SAR is side-view imaging so that terrain undulations can cause geometric distortions to the image [Minh et al., 2019]. For multi-temporal analysis, the topographic correction of the images for each period was performed using the Range-Doppler method in the terrain correction tool of the SNAP data processing software in combination with the SRTM 30 m resolution DEM data.

6. Image alignment. In order to realize the monitoring of dynamic changes of floods based on the same area, the images of two periods need to be accurately aligned. Since the GRD images are in wide interferometric format, they have already been corrected for multi-view and geocoding and do not require further alignment processing.

7. Convert bands to Db. To better reflect the variability of radar intensity and highlight the differences between water and land, the backscattered coefficients of the images are transformed into a logarithmic scale form [Silveira, Heleno, 2009]. The decimalization of the radar backscattered coefficients approximates the standard Gaussian distribution in the data range, which is more convenient for visualization and data analysis. Comparing the pre-processed images (Fig. 3b) with the original ones (Fig. 3a), it can be seen that the contrast between water and land is significantly enhanced in the logarithmic map.

Object-oriented Flooded Area Extraction. Object-oriented classification technology is an information extraction technology based on the target object, using the object after image segmentation as the basis for classification [Clark, Pellikka, 2009]. Then find and extract the target object features from the image and rely on the library of object feature knowledge to complete the extraction of the target object. Traditional

image element-based classification often influences speckle noise. Object-oriented classification technology, which overcomes the shortcomings of traditional remote sensing image classification methods, can improve the efficiency and quality of image interpretation to a certain extent. In this study, based on eCognition software, the object-oriented method extracts the flooded area in the study area.

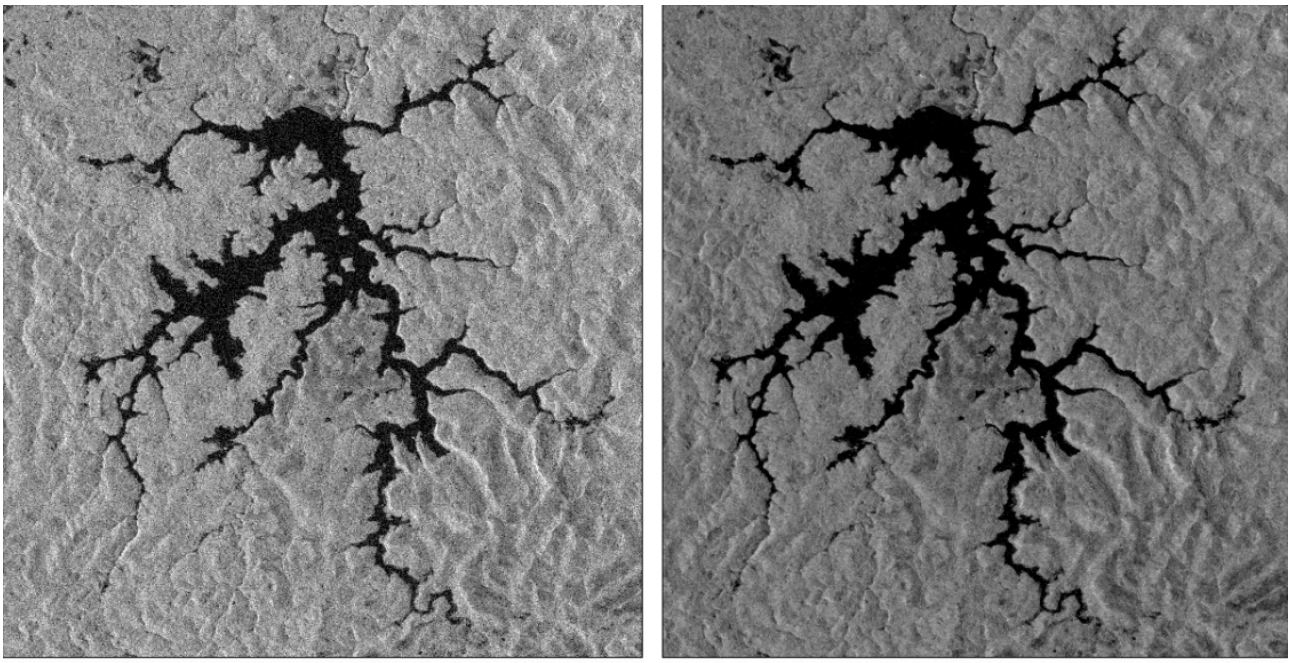

Fig. 3. Original image and pre-processed image of flood on July 13, 2018

Рис. 3. Исходный и предварительно обработанный снимки наводнения от 13 июля 2018 г.

Image Segmentation. Object-oriented classification is the technique of image segmentation, which has a vital role in image information extraction [Lewinski, Zaremski, 2004]. This study uses a multi-scale approach for image segmentation, which refers to segmentation image object levels at different scales by adopting different segmentation scales to generate a hierarchical image mesh structure composed of data at different scales. Multi-scale segmentation can extract image object prototypes without knowledge participation at any scale according to local contrast. It is applied to various data types and can handle multi-channel data, especially for data with texture or low-contrast images with slight differences [Drăguţ et al., 2014]. The multi-scale segmentation algorithm is mainly determined by segmentation parameters such as image band weights, segmentation scale, color, and shape [Lowe, Guo, 2011].

The multi-scale segmentation method needs to be debugged several times to select the optimal segmentation parameters to ensure that the generated image objects have the minimum internal and inter-object heterogeneity. The image objects can sufficiently express the basic features of each object. The heterogeneity is calculated as follows:

$$f = \omega_1 \times h_1 + (1 - \omega_1) \times h_2 \quad (1)$$

where ω_1 is the user-specified shape weight, h_1 is the shape heterogeneity, h_2 is the spectral heterogeneity. The formula for h_1 and h_2 is:

$$\begin{aligned} h_1 &= \omega_2 k_1 + (1 - \omega_2) k_2 \\ h_2 &= \sum_{i=1}^{n} \lambda_i \times \sigma_i \end{aligned} \quad (2)$$

where ω_2 is the user-specified tightness weight, k_1 and k_2 are the tightness and smoothness of the shape, respectively, n is the total number of bands, λ_i is the band weight, and σ_i is the standard deviation of the bands. k_1 and k_2 are calculated as follows:

$$\begin{cases} k_1 = \frac{E}{\sqrt{N}} \\ k_2 = \frac{E}{L} \end{cases} \quad (3)$$

where E is the length of the object boundary, E is the total number of pixels within the object, and L is the perimeter of the rectangle containing the object.

Spectral color and shape are complementary, and if only the spectral color factor is considered, the influence

of the shape factor on the homogeneity criterion is necessarily reduced [Lucas et al., 2007]. Both tightness and smoothness determine the shape, and the ones are also complementary. Increasing the scale factor of smoothness can make the edges of the object smooth, which is very effective for segmenting strip features such as roads; increasing tightness can make the object more rectangular, which is very effective for segmenting images of features with regular shapes. The image segmentation directly affects the accuracy of image classification. In order to obtain the optimal segmentation scale so that the segmented objects can achieve a better fit with the actual feature patches, the appropriate setting of the parameter weights is extremely important;

Knowledge base construction and classification extraction. After determining the appropriate scale of image segmentation, a knowledge base of multiple feature sets must be established. Suitable expressions must be selected to describe the features of the features, that is, to transform this semantic knowledge into rules to achieve the extraction of flooded areas. The establishment of the knowledge base needs to consider the differences between the object to be extracted and the original image, which are reflected in texture, brightness, density, area, and other features. The land-use types in the study area are mainly bare land and residential land. Under the VH polarization, the image's overall brightness is higher, and the distinction between the flooded area and the background area is more apparent. The water features are more stable in the backscattering characteristics of the VH polarization, with less texture information.

In contrast, under the VV polarization mode, there are more apparent variations in the backscattering intensity of some land types, leading to corresponding disturbances in the changes of flooded areas. After sensitivity analysis of the flooded area images and other features, the VH-polarized backscattered mean features are selected to construct a knowledge base for extracting flooded areas to distinguish water bodies from non-water bodies. Since the water body features are straightforward to distinguish on SAR images, this paper uses the threshold method to extract water bodies after multi-scale segmentation.

Results and analysis

Based on the characteristics of the image itself and the research purpose of extracting the flood inundation extent, this study divides the image feature type into inundated and unflooded areas and extracts. It analyzes the flood inundation extent by combining the changes of waters in different periods. Different segmentation results are obtained by adjusting the image segmentation ratio, shape factor, and tightness factor several times, and the best segmentation parameters are selected using a priori knowledge and expert discriminative ability. After screening, the final parameters were set as follows: the scale parameter of image segmentation was set to 15, the shape factor was set to 0.3, the tightness factor was set to 0.5, and the spectral factor was kept as default. The segmentation results obtained according to the above parameters are satisfactory, reflecting the information of the differences between patches, high internal homogeneity of the images, and apparent boundary separation between land and water, maintaining the integrity of the boundary. By analyzing the VH polarization mean features, the average backscattering coefficient of the water body is lower than –17.5 dB. The threshold range is set based on the Assign Class function of eCognition software to extract the water body and non-water body regions.

The SAR image is oblique distance imaging, due to the influence of imaging mechanism, when the electromagnetic wave irradiates to the surface, the mountain in the study area will appear the phenomenon of perspective contraction, superimposed obscuration and shadowing, and the back mountain slope with large topographic undulations in the scene cannot obtain the radar beam and produce mountain shadowing [Sun et al., 2014]. The shaded area has low brightness, and the shadows are similar to the backscattering intensity of water bodies, so the object-oriented threshold-based method cannot completely distinguish the shadows, which may lead to the mountain shadows being misrepresented as water bodies. In response to the problem mentioned above of false information is-extraction, this study uses DEM data to calculate the topographic relief according to the mountain features in the study area and combines the mountain shadow map and incidence angle map to determine the topographic relief threshold of 30m, and extracts the areas with sizeable topographic relief to eliminate the influence of mountain shadow on the extraction results of water bodies. This step can be very effective in removing noise from areas with significant differences in elevation in the study area. Combining the high-resolution images of Landsat 8 and Google Earth of the same period and expert interpretation, it is found that the pre-disaster land-use types of the study area are mainly bare land and inhabited land before the dam collapsed, so most of the Hinlat area is dark in the SAR amplitude image. This phenomenon is since the backscattering coefficient varies depending on soil moisture and surface roughness, which are usually proportional to soil moisture and surface roughness. Since most of the Hinlat area has few structures such as buildings or trees, its surface roughness is low, resulting in a low backscatter coefficient [Kim, Lee, 2020]. The primary land features

behave similarly to water bodies in the backscattering characteristics of VH polarization, which leads to the corresponding disturbance in the changes of the flooded area. It is difficult to distinguish between water bodies and bare soil using a single SAR magnitude image when no other data source is available. Therefore, in this paper, after removing the influence of mountain shadows on the extraction results of water bodies, the modified bare soil index (MBI) [Nguyen et al., 2021] of the study area was calculated using Landsat 8 remote sensing images of the same period. In order to distinguish between bare soil and areas inundated by dam collapse, the MBI threshold was determined to be 0.175 through constant adjustment and variation.

Based on the above research methods, the results of pre-and post-disaster monitoring of Xe-Pian Xe-Namnoy reservoir and flooded villages were obtained (Figs. 4 and 5).

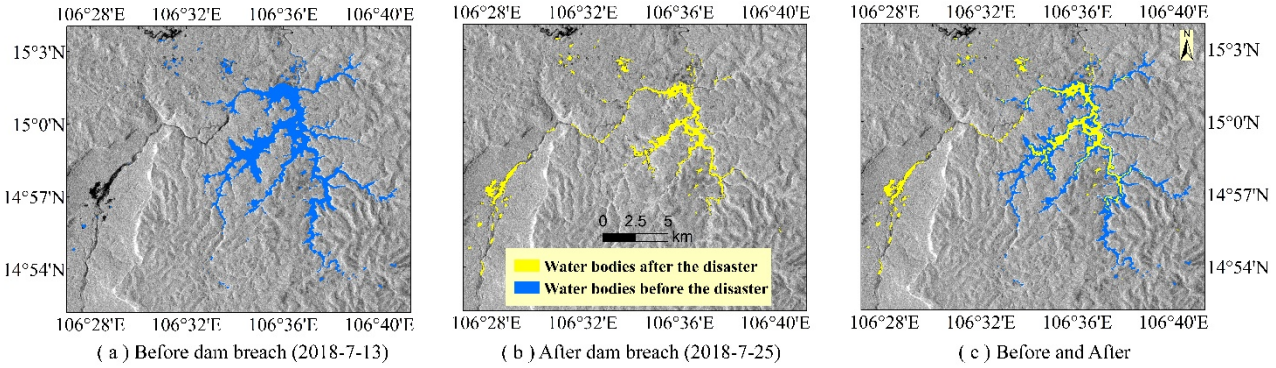

Fig.4. The flooding area extraction results of the Xe-Pian Xe-Namnoy reservoir

Рис.4. Результаты моделирования затопленных территорий в районе водохранилища Xe-Pian Xe-Namnoy

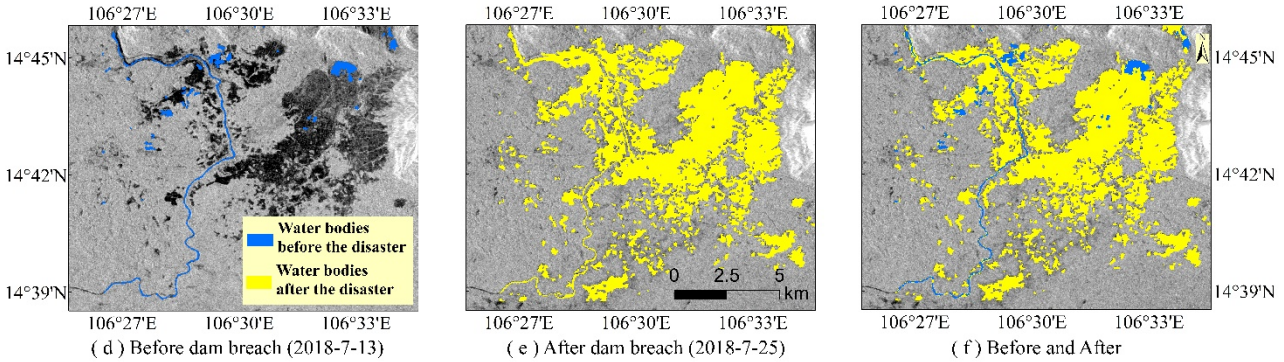

Fig. 5. The flooding area extraction results of the flooded villages

Рис. 5. Результаты моделирования затопленных территорий в районе сельских населенных пунктов

The pre-disaster water body area of the Xe-Pian Xe-Namnoy reservoir is 30.31 km², the water system develops mainly in a southwestern direction, but also occurs in all other directions. The post-disaster water body area is 9.06 km². Comparing with the post-disaster image on July 25, the area of the lost water body on July 13 was 21.25 km², and the area of the water body in the Xe-Pian Xe-Namnoy reservoir before and after the disaster shrank significantly. When we look at the north-south direction of the image, we can see that most of the water stored on the right side of the water system has been released, and the water system in the area has become significantly smaller, with a large amount of water flowing out to the southwest. In the direction south of the reservoir, the water leaking from the reservoir flows along the Vang Nagao River, causing significant damage to the Hinlat area. Figure 4 shows the affected area, the total area of the study area is 190.04 km², the area of the water body before the disaster is 3.28 km², and the area of the water body after the disaster is 51.56 km². Comparing with the pre-disaster image on July 13, the total inundated area on July 25 was 48.66 km². The spa-

tial and temporal distribution of flooding shows that Hinlat, Thasaengchan, Mai, and Samong-tai are more severely affected, concentrated inundation. The interval between the image of the affected period and the image of the post-disaster period is 12 d. Comparing the area of water bodies before and after the disaster, it is clear that the preceding cycle of the marginal area of the site is longer.

The study area is dominated by bare land and residential land, and the terrain is lower than the surrounding area, and the prolonged and continuous heavy rainfall causes the water to be difficult to drain for a short period. As shown in Figure 4, the spatial distribution of the inundated area is relatively concentrated, and the area of the extracted water bodies matches the area of the original image water bodies. Due to the complex changes in the distribution of water bodies in the study area, it is difficult to depict the water body boundaries manually, so this paper combined Landsat 8 and Google Earth high-resolution images before and after the disaster to manually depict the water body boundaries in some areas before the disaster and evaluated the accuracy. The overall accuracy reached 85.9 %.

Discussion and conclusion

In this study, we used eCognition software as a platform to achieve the extraction of water body information from the pre-disaster and post-disaster Sentinel-1A SAR images of the study area by using object-oriented multi-scale segmentation and thresholding method, combined with terrain relief and MBI, and this method was fast and accurate, and good results were obtained. Compared with traditional methods based on image elements, object-oriented classification methods extract homogeneous objects for classification, in which there are relatively few fragmented objects, and merge noisy regions and surrounding objects into a specific object with significantly stronger resistance to noise, which can effectively avoid the "pretzel phenomenon" often generated in image-oriented classification methods.

Due to the limitations of the conditions, the verification of the extraction results for the flooded area lacked the survey data of the actual points in the field, and the continuous cloudy and rainy days during the occurrence of the flood were disturbed by the cloud cover so that the valid high-resolution optical images could not be obtained for the verification analysis of the affected area. The extraction accuracy needed to be further improved.

Influenced by remote sensing data's temporal and spatial resolution, it is difficult to achieve accurate flood monitoring by a single remote sensing data source. Therefore, to carry out multi-source remote sensing data fusion, make full use of the advantages of various data sources, establish multi-source remote sensing flood disaster monitoring response mechanism, improve the corresponding speed of flood disaster monitoring, and then realize the daily supervision of water resources of rivers in the domain and emergency monitoring of unexpected disasters, is the focus of further research on flood monitoring.

References

Campbell I.C. The Mekong: biophysical environment of an international river basin. Academic Press is an imprint of Elsevier, 2009. 432 p.

Cheng S., Zhao W., Yin Z. PS-InSAR Analysis of Collapsed Dam and Extraction of Flood Inundation Areas in Laos Using Sentinel-1 SAR Images // 2019 IEEE 4th Advanced Information Technology, Electronic and Automation Control Conference (IAEAC).: IEEE, 2019. pp. 2605–2608.

Clark B. J., Pellikka P.K. Landscape analysis using multi-scale segmentation and object-oriented classification // Recent advances in remote sensing and geoinformation processing for land degradation assessment.: CRC press, 2009. pp. 343–362.

Delang C., Toro M. Hydropower-induced displacement and resettlement in the Lao PDR // South East Asia Research. 2011. V. 19. pp. 567–594.

Domeneghetti A., Schumann G. J.-P., Tarpanelli A. Preface: Remote Sensing for Flood Mapping and Monitoring of Flood Dynamics // Remote Sensing. 2019. V. 11. No. 8. pp. 943.

Drăguţ L., Csillik O., Eisank C., Tiede D. Automated parameterisation for multi-scale image segmentation on multiple layers // ISPRS Journal of photogrammetry and Remote Sensing. 2014. V. 88. pp. 119–127.

ESA. Sentinel-1 Missions Sentinel Online [Electronic resource]. URL: https://sentinels.copernicus.eu/web/sentinel/missions/sentinel-1. (Date of accessed: 15.09.2021).

Guo X., Zhao Y.D. Floodinundation Monitoring in Ningxiang of Hunan Province based on Sentinel-1A SAR // Remote Sensing Technology and Application. 2018. V. 33. No. 4. pp. 646–656. In Chinese

Han C.M., Guo H.D., Wang C.L. The essence of SAR image speckle suppression // JOURNAL OF REMOTE SENSING-BEIJING. 2002. V. 6, No. 6. pp. 474–479.

Hess L.L., Melack J.M., Filoso S., Wang Y. Delineation of inundated area and vegetation along the Amazon floodplain with the SIR-C synthetic aperture radar // IEEE transactions on geoscience and remote sensing. 1995. V. 33. No. 4. pp. 896–904.

Jain S.K., Saraf A.K., Goswami A., Ahmad T. Flood inundation mapping using NOAA AVHRR data // Water Resources Management. 2006. V. 20, No. 6. pp. 949–959.

Khromykh V.V., Khromykh O.V. Spatial structure and dynamics of Tom river floodplain landscapes based on GIS, digital elevation model and remote sensing // Riparian zones: Characteristics, management practices and ecological impacts. Ed. O.S. Pokrovsky. New York: Nova Science Publishers, 2016. Chapter 12. pp. 289–309.

Khromykh V.V., Khromykh O.V. A study of natural and anthropogenic changes of soils within the Tom river valley based on GIS, remote sensing and field observations // Journal of Physics. IOP Conference Series: Earth and Environmental Science. V. 201. 2018. 012006.

Kiage L.M., Walker N.D., Balasubramanian S., Babin A., Barras J. Applications of Radarsat-1 synthetic aperture radar imagery to assess hurricane-related flooding of coastal Louisiana // International Journal of Remote Sensing. 2005. V. 26. No. 24. pp. 5359–5380.

Kim Y., Lee M.-J. Rapid Change Detection of Flood Affected Area after Collapse of the Laos Xe-Pian Xe-Namnoy Dam Using Sentinel-1 GRD Data // Remote Sensing. 2020. V. 12. No. 12. pp. 1978.

Latrubesse E.M., Park E., Sieh K., Dang T., Lin Y.N., Yun S. Dam failure and a catastrophic flood in the Mekong basin (Bolaven Plateau), southern Laos, 2018 // Geomorphology. 2020. V. 362. pp. 1–16.

Lewinski S., Zaremski K. Examples of object-oriented classification performed on high-resolution satellite images // Miscellanea geographica. 2004. V. 11. pp. 349–358.

Lowe S.H., Guo X.L. Detecting an optimal scale parameter in object-oriented classification // IEEE Journal of Selected Topics in Applied Earth Observations and Remote Sensing. 2011. V. 4. No. 4. pp. 890–895.

Lucas R., Rowlands A., Brown A., Keyworth S., Bunting P. Rule-based classification of multi-temporal satellite imagery for habitat and agricultural land cover mapping // ISPRS Journal of photogrammetry and remote sensing. 2007. V. 62. No. 3. pp. 165–185.

McFeeters S.K. The use of the Normalized Difference Water Index (NDWI) in the delineation of open water features // International journal of remote sensing. 1996. V. 17. No. 7. pp. 1425–1432.

Minh H. V. T., Avtar R., Mohan G., Misra P., Kurasaki M. Monitoring and mapping of rice cropping pattern in flooding area in the Vietnamese Mekong delta using Sentinel-1A data: A case of an Giang province // ISPRS International Journal of Geo-Information. 2019. V. 8. No. 5. pp. 211.

Nandi I., Srivastava P.K., Shah K. Floodplain mapping through support vector machine and optical/infrared images from Landsat 8 OLI/TIRS sensors: case study from Varanasi // Water Resources Management. 2017. V. 31. No. 4. pp. 1157–1171.

Nguyen C.T., Chidthaisong A., Kieu D.P., Huo L.Z. A Modified Bare Soil Index to Identify Bare Land Features during Agricultural Fallow-Period in Southeast Asia Using Landsat 8 // Land. 2021. V. 10. No. 3. pp. 231.

Ouyang Y., Liu H., Wang X., Liu S, Zhang J., Gao H. Spatial Distribution Prediction of Laterite Bauxite in Bolaven Plateau Using GIS // Journal of Earth Science. 2019. V. 30. No.5. pp. 1010–1019.

Ramsey E., Lu Z., Suzuoki Y., Rangoonwala A., Werle D. Monitoring duration and extent of storm-surge and flooding in western coastal Louisiana marshes with Envisat ASAR data // IEEE Journal of Selected Topics in Applied Earth Observations and Remote Sensing. 2011. V. 4. No. 2. pp. 387–399.

Sakamoto T., Van N.N., Kotera A., Ohno H., Ishitsuka N., Yokozawa M. Detecting temporal changes in the extent of annual flooding within the Cambodia and the Vietnamese Mekong Delta from MODIS time-series imagery // Remote Sensing of Environment. 2007. V. 109. No. 3. pp. 295–313.

Schlaffer S., Matgen P., Hollaus M., Wagner W. Flood detection from multi-temporal SAR data using harmonic analysis and change detection // International Journal of Applied Earth Observation and Geoinformation. 2015. V. 38. pp. 15–24.

Sharitz R. Remote sensing inland wetlands: a multispectral approach // Photogrammetric Engineering and Remote Sensing. 1986. V. 52. No. 1. pp. 87–100.

Sieh K., Herrin J., Jicha B., Schonwalder-Angel D., Moore J.D.P., Banerjee P., Wiwegwin W., Sihavong V., Singer B., Chualaowanich T., Charusiri P. Australasian impact crater buried under the Bolaven volcanic field, Southern Laos // PNAS. 2020. V. 117. pp. 1346–1353.

Silveira M., Heleno S. Separation between water and land in SAR images using region-based level sets // IEEE Geoscience and Remote Sensing Letters. 2009. V. 6. No 3. pp. 471–475.

Sun Y.Y., Li X.T., Yang F.J., Huang S.F. Study on the method of mountain water extraction based on the space- borne SAR images // China Institute of Water Resources and Hydropower Research. 2014. V. 12. No. 3. pp. 258–263.

Sun Y.Y., Huang S.F., Li J.R., Li X.T, Ma J.W., Qu W. The Downstream Flood Monitoring Application of Myan-mar Irrawaddy River based on Sentinel-1A SAR // Remote Sensing Technology and Application. 2017. V. 32. No. 2. pp. 282–288. In Chinese

Tang L.Y., Liu W., Yang D., Chen L., Su Y.M., Xu X.L. Flooding monitoring application based on the object-oriented method and Sentinel-1A SAR data // Journal of Geo-information Science. 2018. V. 20. No. 3. pp. 377–384. In Chinese

The Weather Year Round Anywhere on Earth. Climate reports with the weather by month, day, even hour. Great for event and trip planning [Electronic resource]. URL: https://weatherspark.com/ (access date: 22.02.2022).

Wood M., de Jong S.M., Straatsma M.W. Locating flood embankments using SAR time series: A proof of concept // International journal of applied earth observation and geoinformation. 2018. V. 70. pp. 72–83.

Xu Y., Zhou Y. Review on SAR image speckle suppression // Computer Engineering and Applications. 2013. V. 49. No. 20. pp. 210–216. In Chinese

Zhang X., Chan N.W., Pan B., Ge X.Y., Yang H. Mapping flood by the object-based method using backscattering coefficient and interference coherence of Sentinel-1 time series // Science of The Total Environment. 2021. V. 794. pp. 148–388.

Information about the authors:
Ma J., Postgraduate Student, Department of Geography, Geology and Geography Faculty, National Research Tomsk State University.
E-mail: majun6982@gmail.com
Khromykh V.V., Cand. Sci. (Geography), Associate Professor, Department of Geography, Geology and Geography Faculty, National Research Tomsk State University, Tomsk, Russia.
E-mail: khromykh_vadim@mail.ru
Chekina A.A., Postgraduate Student, Department of Geography, Geology and Geography Faculty, National Research Tomsk State University, Tomsk, Russia.
E-mail: chekina.ann@gmail.com

The authors declare no conflicts of interests.

Информация об авторах:
Ма Д., аспирант, кафедра географии, геолого-географический факультет, Национальный исследовательский Томский государственный университет, Томск, Россия.
E-mail: majun6982@gmail.com
Хромых В.В., кандидат географических наук, доцент, кафедра географии, геолого-географический факультет, Национальный исследовательский Томский государственный университет, Томск, Россия.
E-mail: khromykh_vadim@mail.ru
Чекина А.А., аспирант, кафедра географии, геолого-географический факультет, Национальный исследовательский Томский государственный университет, Томск, Россия.
E-mail: chekina.ann@gmail.com

Авторы заявляют об отсутствии конфликта интересов.

Статья поступила в редакцию 30.03.2022; одобрена после рецензирования 29.06.2022; принята к публикации 12.09.2022

The article was submitted 30.03.2022; approved after reviewing 29.06.2022; accepted for publication 12.09.2022